This is the accepted manuscript made available via CHORUS. The article has been published as:

Temperature-driven evolution of critical points, interlayer coupling, and layer polarization in bilayer MoS_{2}

Luojun Du, Tingting Zhang, Mengzhou Liao, Guibin Liu, Shuopei Wang, Rui He, Zhipeng Ye, Hua Yu, Rong Yang, Dongxia Shi, Yugui Yao, and Guangyu Zhang

Phys. Rev. B **97**, 165410 — Published 9 April 2018

DOI: 10.1103/PhysRevB.97.165410

Temperature-driven evolution of critical points, interlayer coupling and layer polarization in Bilayer MoS_2

Luojun Du[1,2†], Tingting Zhang[1†], Mengzhou Liao[1], Guibin Liu[3], Shuopei Wang[1], Rui He[4], Zhipeng Ye[4], Hua Yu[1], Rong Yang[1], Dongxia Shi[1,5,6]*, Yugui Yao[3], Guangyu Zhang[1,5,6,7]*

[1]Beijing National Laboratory for Condensed Matter Physics and Institute of Physics, Chinese Academy of Sciences, Beijing 100190, China

[2]Department of Physics, Beijing Key Laboratory of Opto-Electronic Functional Materials and Micro-nano Devices, Renmin University of China, Beijing 100872, China

[3]Beijing Key Laboratory of Nanophotonics and Ultrafine Optoelectronic Systems, School of Physics, Beijing Institute of Technology, Beijing 100081, China

[4]Department of Electrical and Computer Engineering, Texas Tech University, Lubbock, Texas 79409, USA

[5]School of Physical Sciences, University of Chinese Academy of Science, Beijing 100190, China

[6]Beijing Key Laboratory for Nanomaterials and Nanodevices, Beijing 100190, China

[7]Collaborative Innovation Center of Quantum Matter, Beijing 100190, China

†These authors contributed equally to this work

*Corresponding authors. E-mail: gyzhang@ iphy.ac.cn; dxshi@iphy.ac.cn

The recently emerging two-dimensional (2D) transition metal dichalcogenides (TMDCs) have been a fertile ground for exploring abundant exotic physical properties. Critical points, the extrema or saddle points of electronic bands, are the cornerstone of condensed-matter physics and fundamentally determine the optical and transport phenomena of the TMDCs. However, for bilayer MoS_2, a typical TMDCs and the unprecedented electrically tunable venue for valleytronics, there has been a considerable controversy on its intrinsic electronic structure, especially for the conduction band edges locations. Moreover, interlayer hopping and layer polarization in bilayer MoS_2 which play vital roles in valley-spintronic applications have remained experimentally elusive. Here, we report the first experimental observation of intrinsic critical points locations, interlayer hopping, layer-spin polarization and their evolution with temperature in bilayer MoS_2 by performing temperature-dependent

photoluminescence (PL). Our measurements confirm that the conduction band minimum locates at the K_c instead of Q_c, and the energy splitting between Q_c and K_c red-shifts with a descent of temperature. Furthermore, the interlayer hopping energy for holes and temperature-dependent layer polarization are quantitatively determined for the first time. Our observations are in good harmony with density functional theory (DFT) calculations.

I. INTRODUCTION

Monolayer TMDCs with inversion asymmetry, strong spin-orbit coupling (SOC) and valley-spin entanglement have offered new opportunities to address a variety of intriguing properties [1–6], such as valley physics [7–9] and unconventional quantum Hall effect [10,11]. Moreover, 2H stacked TMDCs bilayers, two equivalent monolayers are rotated by π with respect to each other [Figs. 1(a) and 1(b)], harbour layer degree of freedom and layer-spin polarization [1]. It thus provides a prefect electrically tunable platform for topological valley transport [12] and magneto-electric effects [13], in which inversion symmetry, Berry curvature and valley magnetic moment [14] can be continuously tuned by a perpendicular electric field. Compared to the theoretical and experimental consensus on the direct-gap in monolayer limit located at the corners of the first Brillouin zone (BZ) [15,16], the electronic structures of TMDCs bilayers are still under debating, in particular the conduction band minimum (CBM) of bilayer MoS_2 [17]. Some indicate that CBM should locate at K points, while the others reveal that CBM is at nonsymmetric Q points [Fig. 1(c)] (Supplemental Material [18]). In addition, Q points are associated with a number of novel valley physics (to name but a few, Q-valley quantum Hall effects [19] and intervalley quantum interference [20]). Thus, it is quite nontrivial to the experimental determination of critical points loci in bilayer MoS_2.

The band structure could be characterized by spectroscopic techniques such as angle-resolved photoemission spectroscopy (ARPES) and scanning tunneling microscopy/spectroscopy (STM/S). ARPES is able to directly observe the electronic structures below Fermi level (valence band of TMDCs) [21,22], while the conduction band can only be determined in heavily-doped samples. Doping could lead to momentum-dependent energy shift and cannot give us the uncontested intrinsic location of critical points [21,23,24]. For STM/S, it is difficult to access the K valley states due to the larger parallel momentum, as compared with Γ and Q valleys [20,25]. Besides, conductive substrates, such as graphite, could also give rise to gigantic bandgap renormalization [26].

PL spectroscopy is another choice due to its high energy resolution and characteristic optical transitions associated with critical points. Recently, Zhao *et al.* investigated the temperature-dependent PL in few-layer TMDCs and have shown two indirect excitons for bilayer WSe_2 [27]. Since the energy of indirect exciton associated with Q_c point is lower than that associated with K_c point, the CBM of bilayer WSe_2 should locate at the Q_c point, in good agreement with the STM/S results [25]. However, only one indirect exciton was observed in bilayer MoS_2 [27]. Thus, the CBM of bilayer MoS_2 cannot be extracted. More importantly, interlayer hopping (LH) and layer-spin polarization of bilayer MoS_2 and their evolution with temperature, which are fundamentally included in magneto-electric effects and quantum gates, have not yet been experimentally addressed. In this Letter, we resolve the previous controversy on CBM in bilayer MoS_2, provide the first firm and clear experimental evidence of LH and layer-spin polarization and uncover how they evolve with temperature from PL spectroscopy.

II. RESULTS AND DISCUSSION

Experiments were performed on three bilayer MoS_2 samples that were mechanically exfoliated from bulk crystals onto SiO_2/silicon substrates. Figure 1(d) shows an optical micrograph of a representative sample. The number of layers is identified by a combination of atomic force microscopy (AFM), Raman modes and PL spectra. The thickness of 1.36 nm [Fig. 1(e)], frequency difference between E_{2g}^1 and A_{1g} modes of 22 cm^{-1} [Fig. 1(f)], shear mode at 22 cm^{-1} and indirect bandgap of 1.6 eV (Supplemental Material [18]) verify that our sample is indeed bilayer.

We first performed DFT calculations (Supplemental Material [18]) for the band structure of bilayer MoS_2 to investigate the orbital compositions of Bloch states at critical points. Figure 2(a) is the calculated energy band. Critical points are located at K_c and Q_c for conduction band, K_{v1}, K_{v2} and Γ_v for valance band. It can be seen that Bloch wavefunctions at K valley are predominantly from Mo-d_{xy},$d_{x^2-y^2}$,d_{z^2} orbitals, with some S-p_x,p_y characters confined within the 2D *xy* plane [Fig. 2(b)]. Therefore, the energy level of critical points in K valley are mainly affected by in-plane lattice constant ***a***. K_c red-shifts, and K_{v1}/K_{v2} blue-shifts when ***a*** increases. While the considerable S-p_z character at Q_c and Γ_v [Fig. 2(b)] leads to significant LH and causes the energy upshifted for Q_c and downshifted for Γ_v as the LH weakening, being akin to the crossover from the indirect-gap in bulk to direct-gap in monolayer.

Four possible transitions between critical points, corresponding to A exciton ($K_c \rightarrow K_{v1}$), B exciton ($K_c \rightarrow K_{v2}$), I_1 exciton ($Q_c \rightarrow \Gamma_v$) and I_2 exciton ($K_c \rightarrow \Gamma_v$), are marked in Fig. 2(a). At low temperatures, we can observe five excitons: trion exciton, A exciton, B exciton [Fig. 2(c)] and coexistence of two indirect-gap excitons [Fig. 2(d)]. This is the first experiment that two indirect-gap transitions of bilayer MoS_2 are observed simultaneously. This result is of particular significance to obtain the loci of critical points, as will be seen in below. The peak positions of B, A and trion excitons are fitted well [solid lines in Fig. 2(e)] using the standard semiconductor bandgap dependence [28] of $E_g(T) = E_g(0) - S\hbar\omega[\coth(\frac{\hbar\omega}{2kT} - 1)]$, where $E_g(0)$ is the ground-state transition energy at 0 K, S, $\hbar\omega$ and k are the dimensionless coupling constant, average phonon energy and Boltzmann constant, respectively. Trion exciton possesses a large binding energy of 27 meV, in line with previous reports [7,29] (Supplemental Material [18]). The two indirect transitions with nearly degenerate energy are indistinguishable between each other from the PL spectra. However, we can discriminate I_1 and I_2 excitons from their evolution with temperature [Fig. 2(f)]. Thermal expansion drives interlayer spacing (***c***) and ***a*** to increase with temperature, thus the energy level of K_c, Γ_v lowers, and the energy level of Q_c point lifts. Therefore, when the temperature rises, I_1 exciton energy should blue-shift monotonically, whereas I_2 energy remains largely unchanged (Supplemental Material [18]). From Fig. 2(f), we can extract that the exciton with higher energy is I_1 exciton and I_2 possesses the lower energy. I_2 exciton data > 150 K is not present as it becomes negligible. The reason for the lack of I_2 exciton at high temperatures is due to that both the direct-gap transitions (A and B excitons) and indirect I_2 exciton are from the K_c point. Rising the temperature can effectively increase the relative quantum yield ratio between direct excitons and I_2 exciton by thermally decoupling neighboring monolayers via interlayer thermal expansion. Thus, at high temperature, electrons at K_c point only recombine with holes at K_v point and I_2 exciton disappears (Supplemental Material [18]). Figures 2(g) and 2(h) show the temperature-dependent evolution of electronic transition energies by DFT calculations with thermal expansion coefficients of bulk MoS_2 [27,30]. In spite of the energy scale difference, the theoretical calculations are in good qualitative agreement with the Bloch states analyses and PL results.

Based on these obtained transitions between critical points, we thus could acquire the critical points loci. Since the indirect transitions should be phonon-assisted, we first consider the phonon effects. The I_1 and I_2 excitons are accompanied by phonons with wave vector **Q** and **K**, respectively due to the momentum conservation (Supplemental Material [18]). Recently, Carvalho *et al.* have demonstrated that the acoustic phonons LA (K) and LA (Q) in MoS_2 are pivotal to the electron-phonon scattering pathways [31]. Thus, we believe that the indirect excitons of I_1 and I_2 should be connected primary by LA (Q) and LA (K) phonons, respectively. As the energy difference between LA (Q) (185 cm^{-1}) and LA (K) (230 cm^{-1}) is only 5.5 meV, the effect of phonon energies can be ignored. Second, we consider the exciton-phonon coupling (EPC) which may play a fundamental role for 2D materials. A recent work has shown that the EPC of MoS_2 decreases with thickness decreasing and only a tiny EPC strength appears in bilayer MoS_2 [32]. Thus, the polaron shift stemmed from EPC makes trivial contributions for bilayer MoS_2. The energy spacing between critical points is associated with excitons and their binding energies [Fig. 2(a)]. The energy splitting between Q_c and K_c:

$$\Delta E(Q_c - K_c) = E(Q_c) - E(K_c) = [E(I_1) - E(I_2)] + [E_b(I_1) - E_b(I_2)] \qquad (1)$$

where the E_b is the binding energy of exciton. In the same way, we can deduce the energy separation between Γ_v and K_{v1}, and between K_{v1} and K_{v2} as following:

$$\Delta E(\Gamma_v - K_{v1}) = [E(A) - E(I_2)] + [E_b(A) - E_b(I_2)] \qquad (2)$$

$$\Delta E(K_{v1} - K_{v2}) = [E(B) - E(A)] + [E_b(B) - E_b(A)] \qquad (3)$$

First, we assume that all excitons harbour the equal binding energy for simplicity. This is reasonable since the binding energies of all excitons are at the same energy scale. And the binding energy does not affect our results as will be discussed below. Therefore, equation 1, 2, 3 can be written into:

$$\Delta E(Q_c - K_c) = E(I_1) - E(I_2) \qquad (4)$$

$$\Delta E(\Gamma_v - K_{v1}) = E(A) - E(I_2) \qquad (5)$$

$$\Delta E(K_{v1} - K_{v2}) = E(B) - E(A) \qquad (6)$$

We can see that the I_2 exciton that has not been observed previously plays a pivotal role in determining the critical points loci.

Figure 3(a) shows the energy difference between A and I_2 excitons versus temperature. At low temperatures, valence band maximum (VBM) is located at the Γ_v and 0.493 eV higher than the K_{v1} point, in fair agreement with cryogenic ARPES measurements (0.5 eV) [22], indicating that the effect of binding energy is trivial and can be ignored. When the temperatures vary from 3 K to 140 K, the energy separation between A and I_2 excitons red-shifts monotonically, in good agreement with previous orbital compositions analyses that the energy level moves down (up) for Γ_v (K_{v1}) point as temperature rising. The energy splitting between I_1 and I_2 excitons is displayed in Fig. 3(c). We deduce that CBM is located at the K_c point due to I_1 exciton possesses larger energy than I_2 exciton, in good agreement with both our DFT calculations. The energy spacing between Q_c and K_c monotonically decreases with temperature dropping and is 40 meV at 3K, in good harmony with previous Bloch wavefunctions analysis that the energy moves down (up) for Q_c (K_c)point with a descent of temperature. Despite a little energy scale difference, theoretical calculations [Figs. 3(b) and 3(d)] and experimental results [Figs. 3(a) and 3(c)] can match very well.

Figure 3(e) presents the energy difference between B and A excitions as a function of temperature. Usually, we believe that the energy separation between B and A excitons is SOC-induced valence band splitting (VBS) [15] and should be independent on temperature. However, both our experimental results [Fig. 3(e)] and theoretical calculations [Fig. 3(f)] show that VBS is getting larger as the temperature gets close to 0 K.

What is the physical origin of temperature-dependent VBS? In fact, VBS consists of two parts: temperature-independent SOC and temperature-dependent LH. The 180° rotation between two adjacent monolayers in 2H stacked bilayer MoS_2 switches the K and K′ valleys, but leaves spin unchanged, leading to spin-layer locking [Fig. 4(a)]. Since LH conserves both spin and lattice momentum, LH between spin-down (spin-up) state of upper layer and spin-up (spin-down) state of lower layer is virtually quenched [dashed black arrows in Fig. 4(a)]. Thus, LH is usually overlooked in previous studies [17,33,34]. However, SOC strength is not infinite (140 meV for MoS_2), LH with energy cost between spin-down (spin-up) state of upper layer and spin-down (spin-up) state of lower layer, marked by the magenta bidirectional arrows in Fig. 4(a), can still occur [35]. These LHs give rise to the widening of VBS ($\mathrm{VBS} = \sqrt{\mathrm{SOC}^2 + \mathrm{LH}^2}$) [13] and lead to the VBS blue-shifts monotonically with decreasing temperature due to the strengthening of interlayer coupling indicated by the Raman shear mode (Supplemental Material [18]). Figures 4(b) and 4(c) present the evolution of VBS versus the change of ***a*** and ***c***. VBS is independent of ***a*** and only affected by ***c***. The stronger the interlayer coupling is, the larger the VBS is, signifying that the evolution of VBS with temperature is caused by the temperature-dependent strength of LH [35].

We then quantify the temperature-dependent LH and the degree of layer-spin polarization (ρ) by [14],

$$\mathrm{LH(T)} = \sqrt{\mathrm{VBS(T)}^2 - \mathrm{SOC}^2} \qquad (7) \qquad \text{and} \qquad \rho(\mathrm{T}) = \frac{\mathrm{SOC}}{\sqrt{\mathrm{SOC}^2 + \mathrm{LH(T)}^2}} \qquad (8)$$

We assume that LH is quenched and SOC is equal to the VBS at 450 K, as interlayer coupling at 450 K is relatively weak and it only has a little effect on the absolute value of LH and layer polarization. Figure 5 presents the LH and layer polarization as a function of temperature. We can deduce that LH increases while layer polarization drops with decreasing temperature. At low temperatures, LH and layer polarization are ~ 100 meV and 75%, respectively, being consistent with recent theoretical calculations [13]. This direct and firm evidence on temperature-dependent LH and layer polarization would play a prominent role in understanding and optimizing the circular dichroism, spin–layer locking effects and valley-spintronic physics in TMDCs bilayers [13,33,36].

Finally, let's take the exciton binding energy into account. The larger electron effective mass would lead to the stronger bound exciton. Binding energy of the direct and indirect excitons harbour the following relationship: $E_b(I_1) > E_b(I_2) > E_b(A) = E_b(B)$, since the effective mass at Q and Γ valleys is found to be larger than that at K valley (Supplemental Material [18]). The largest binding energy of I_1 exciton only enlarges the energy spacing between Q_c and K_c (equation 1). The CBM is not affected by the binding energy and still at K_c point. In addition, the binding energy for A exciton is the same with B exciton and has little impact on VBS and layer-spin polarization.

III. CONCLUSION

To summarize, we have successfully resolved the controversy on the CBM in bilayer MoS_2 and demonstrated, for the first time, the evolution of critical points loci, interlayer hopping and layer polarization with temperature. We quantitatively determined the interlayer hopping for holes on the order of 100 meV at low temperature and temperature-dependent layer polarization. Our work will shed lights on the understanding and engineering of valley-controlled spin quantum logic in bilayer MoS_2, and provide an effective and versatile means to determine the critical points loci with nearly degenerate energy, SOC-dependent interlayer hopping and layer polarization in 2D semiconductors.

Acknowledgements

We acknowledge Feng Wang from UC Berkeley and Marek Potemski from Laboratoire National des Champs Magnétiques Intenses for valuable discussions. GYZ thanks the supports from the National Key R&D program under Grant No. 2016YFA0300904, the National Science Foundation of China (NSFC, Grant No. 61325021), the Key Research Program of Frontier Sciences of the Chinese Academy of Sciences (CAS, Grant No. QYZDB-SSW-SLH004), and the Strategic Priority Research Program (B) of CAS (Grant Nos. XDPB0602 and XDB07010100). DXS thanks the support from NSFC with the Grant No. 51572289. RY thanks the supports from the National 973 program (Grant No.2013CBA01602), NSFC with the Grant No. 11574361. R.H. acknowledges support by the CAREER Grant from the NSF of the U.S. (Grant No. DMR-1760668).

References

[1] X. Xu, W. Yao, D. Xiao, T. F. Heinz, Spin and pseudospins in layered transition metal dichalcogenides, Nat. Phys. **10,** 343 (2014).

[2] E. J. Sie, C. H. Lui, Y-H. Lee, L. Fu, J. Kong, N. Gedik, Large, valley-exclusive Bloch-Siegert shift in monolayer WS_2, Science **355,** 1066 (2017).

[3] K. L. Seyler, J. R. Schaibley, P. Gong, P. Rivera, A. M. Jones, S.Wu, J. Yan, D. G. Mandrus, W. Yao, X. Xu, Electrical control of second-harmonic generation in a WSe_2 monolayer transistor, Nat. Nanotech. **10,** 407 (2015).

[4] J. Xiao, Z. Ye, Y. Wang, H. Zhu, Y. Wang, X. Zhang, Nonlinear optical selection rule based on valley-exciton locking in monolayer WS_2, Light Sci. Appl. **4,** e366 (2015).

[5] A. M. Jones, H. Yu, N. J. Ghimire, S. Wu, G. Aivazian, J. S. Ross, B. Zhao, J. Yan, D. G. Mandrus, D. Xiao, W. Yao, X. Xu, Optical generation of excitonic valley coherence in monolayer WSe_2, Nat. Nanotech. **8,** 634 (2013).

[6] K. Hao, G. Moody, F. Wu, C. K. Dass, L. Xu, C-H. Chen, L. Sun, M-Y. Li, L-J. Li, A. H. MacDonald, X. Li, Direct measurement of exciton valley coherence in monolayer WSe_2, Nat. Phys. **12,** 677-682 (2016).

[7] K. F. Mak, K. He, J. Shan, T. F. Heinz, Control of valley polarization in monolayer MoS_2 by optical helicity, Nat. Nanotech. **7,** 494 (2012).

[8] H. Zeng, J. Dai, W. Yao, D. Xiao, X. Cui, Valley polarization in MoS_2 monolayers by optical pumping, Nat. Nanotech. **7,** 490 (2012).

[9] A. Srivastava, M. Sidler, A. V. Allain, D. S. Lembke, A. Kis, A. Imamoğlu, Valley Zeeman effect in elementary optical excitations of monolayer WSe_2, Nat. Phys. **11,** 141 (2015).

[10] K. F. Mak, K. L. McGill, J. Park, P. L. McEuen, The valley Hall effect in MoS_2 transistors, Science **344,** 1489 (2014).

[11] X. Li, F. Zhang, Q. Niu, Unconventional Quantum Hall Effect and Tunable Spin Hall Effect in Dirac Materials: Application to an Isolated Trilayer, Phys. Rev. Lett. **110,** 066803 (2013).

[12] J. Lee, K. F. Mak, J. Shan, Electrical control of the valley Hall effect in bilayer MoS_2 transistors, Nat. Nanotech. **11,** 421 (2016).

[13] Z. Gong, G-B. Liu, H. Yu, D. Xiao, X. Cui, X. Xu, W. Yao, Magnetoelectric effects and valley-controlled spin quantum gates in transition metal dichalcogenide bilayers, Nat. Commun. **4,** 2053 (2013).

[14] S. Wu, J. S. Ross, G-B. Liu, G. Aivazian, A. Jones, Z. Fei, W. Zhu, D. Xiao,W. Yao, D. Cobden, X. Xu, Electrical tuning of valley magnetic moment through symmetry control in bilayer MoS_2, Nat. Phys. **9**, 149 (2013).

[15] A. Splendiani, L. Sun, Y. Zhang, T. Li, J. Kim, C-Y. Chim, G. Galli, F. Wang, Emerging Photoluminescence in Monolayer MoS_2, Nano Lett. **10,** 1271 (2010).

[16] K. F. Mak, C. Lee, J. Hone, J. Shan, T. F. Heinz, Atomically Thin MoS_2: A New Direct-Gap Semiconductor, Phys. Rev. Lett. **105,** 136805 (2010).

[17] G-B. Liu, D. Xiao, Y. Yao, X. Xu, W. Yao, Electronic structures and theoretical modelling of two-dimensional group-VIB transition metal dichalcogenides, Chem. Soc. Rev. **44,** 2643 (2015).

[18] See Supplemental Material for details on controversy about the electronic structure of TMDCs bilayer, sample preparation and measurements, layer-dependent PL spectra, theory

calculations, temperature-dependent PL of additional bilayer MoS_2, temperature-independent trion binding energy, temperature-dependent shear mode, the effective mass at critical points, and temperature-dependent indirect transitions intensity. This includes Refs. [13, 15, 16, 23, 27, 29, 30, 37-62].

[19] Z.Wu, S. Xu, H. Lu, A. Khamoshi, G-B. Liu, T. Han, Y Wu, J. Lin, G. Long, Y. He, Y. Cai, Y. Yao, F. Zhang, N. Wang, Even–odd layer-dependent magnetotransport of high-mobility Q-valley electrons in transition metal disulfides, Nat. Commun. **7,** 12955 (2016).

[20] H. Liu, J. Chen, H. Yu, F. Yang, L. Jiao, G-B. Liu, W. Ho, C. Gao, Jinfeng Jia, W. Yao, M. Xie, Observation of intervalley quantum interference in epitaxial monolayer tungsten diselenide, Nat. Commun. **6,** 8180 (2015).

[21] Y. Zhang, T-R. Chang, B. Zhou, Y-T. Cui, H. Yan, Z. Liu, F. Schmitt, J. Lee, R. Moore, Y. Chen, H. Lin, H-T. Jeng, S-K. Mo, Z. Hussain, A. Bansil, Z-X Shen, Direct observation of the transition from indirect to direct bandgap in atomically thin epitaxial $MoSe_2$, Nat. Nanotech. **9,** 111 (2014).

[22] H. Yuan, Z. Liu, G. Xu, B. Zhou, S. Wu, D. Dumcenco, K. Yan, Y. Zhang, S-K. Mo, P. Dudin, V. Kandyba, M. Yablonskikh, A.Barinov, Z. Shen, S. Zhang, Y. Huang, X. Xu, Z. Hussain, H. Y. Hwang, Y. Cui, Y. Chen, Evolution of the valley position in bulk transition-metal chalcogenides and their monolayer limit, Nano Lett. **16,** 4738 (2016).

[23] Y. Zhang, M. M. Ugeda, C. Jin, S-F. Shi, A. J. Bradley, A. Martín-Recio, H. Ryu, J. Kim, S. Tang, Y. Kim, B. Zhou, C. Hwang, Y. Chen, F. Wang, M. F. Crommie, Z. Hussain, Z-X. Shen, S-K. Mo, Electronic Structure, Surface Doping, and Optical Response in Epitaxial WSe_2 Thin Films, Nano Lett. **16,** 2485 (2016).

[24] M. Kang, B. Kim, S. H. Ryu, S. W. Jung, J. Kim, L. Moreschini, C. Jozwiak, E. Rotenberg, A. Bostwick, K. Su Kim, Universal mechanism of band-gap engineering in transition-metal dichalcogenides, Nano Lett. **17,** 1610 (2017).

[25] C. Zhang, Y. Chen, A. Johnson, M-Y. Li, L-J. Li, P. C. Mende, R. M. Feenstra, C-K. Shih, Probing Critical Point Energies of Transition Metal Dichalcogenides: Surprising Indirect Gap of Single Layer WSe_2, Nano Lett. **15,** 6494 (2015).

[26] M. M. Ugeda, A. J. Bradley, S-F.Shi, F. H. da Jornada, Y. Zhang, D. Y. Qiu,W. Ruan, S-K. Mo, Z. Hussain, Z-X. Shen, F. Wang, S. G. Louie, M. F. Crommie, Giant bandgap renormalization

and excitonic effects in a monolayer transition metal dichalcogenide semiconductor, Nat. Mater. **13,** 1091 (2014).

[27] W. Zhao, R. M. Ribeiro, M. Toh, A. Carvalho, C. Kloc, A. Castro Neto, G. Eda, Origin of Indirect Optical Transitions in Few-Layer MoS_2, WS_2, and WSe_2, Nano Lett. **13,** 5627 (2013).

[28] K. O'Donnell, X. Chen, Temperature dependence of semiconductor band gaps, Appl. Phys. Lett. **58,** 2924 (1991).

[29] K. F. Mak, K. He, C. Lee, G. H. Lee, J. Hone, T. F. Heinz, J. Shan, Tightly bound trions in monolayer MoS_2, Nat. Mater. **12,** 207 (2013).

[30] R. Murray, B. Evans, The thermal expansion of 2H-MoS_2 and 2H-WSe_2 between 10 and 320 K, J. Appl. Crystallogr. **12,** 312 (1979).

[31] B. R. Carvalho, Y. Wang, S. Mignuzzi, D. Roy, M. Terrones, C. Fantini, V. H. Crespi, L. M. Malard, M. A. Pimenta, Intervalley scattering by acoustic phonons in two-dimensional MoS_2 revealed by double-resonance Raman spectroscopy, Nat. Commun. 8, 14670 (2017).

[32] B. R. Carvalho, L. M. Malard, J. M. Alves, C. Fantini, M. A. Pimenta, Symmetry-Dependent Exciton-Phonon Coupling in 2D and Bulk MoS_2 Observed by Resonance Raman Scattering, Phys. Rev. Lett. 114, 136403 (2015).

[33] B. Zhu, H. Zeng, J. Dai, Z. Gong, X. Cui, Anomalously robust valley polarization and valley coherence in bilayer WS_2, Proc. Natl Acad. Sci. USA **111,** 11606 (2014).

[34] A. M. Jones, H. Yu, J. S. Ross, P. Klement, N. J. Ghimire, J. Yan, D. G. Mandrus,W. Yao, X. Xu, Spin–layer locking effects in optical orientation of exciton spin in bilayer WSe_2, Nat. Phys. **10,** 130 (2014).

[35] X. Fan, D. J. Singh, W. Zheng, Valence Band Splitting on Multilayer MoS_2: Mixing of Spin−Orbit Coupling and Interlayer Coupling. J. Phys. Chem. Lett. **7**, 2175 (2016).

[36] Q. Liu, X. Zhang, A. Zunger, Intrinsic Circular Polarization in Centrosymmetric Stacks of Transition-Metal Dichalcogenide Compounds, Phys. Rev. Lett. 114, 087402 (2015).

[37] S. Lebegue, O. Eriksson, Electronic structure of two-dimensional crystals from ab initio theory, Phys. Rev. B **79,** 115409 (2009).

[38] K. Kośmider, J. W. González, J. Fernández-Rossier, Large spin splitting in the conduction band of transition metal dichalcogenide monolayers, Phys. Rev. B **88,** 245436 (2013).

[39] T. Cheiwchanchamnangij, W. R. Lambrecht, Quasiparticle band structure calculation of monolayer, bilayer, and bulk MoS_2, Phys. Rev. B **85,** 205302 (2012).

[40] A. Ramasubramaniam, Large excitonic effects in monolayers of molybdenum and tungsten dichalcogenides, Phys. Rev. B **86,** 115409 (2012).

[41] L. Debbichi, O. Eriksson, S. Lebègue, Electronic structure of two-dimensional transition metal dichalcogenide bilayers from ab initio theory, Phys. Rev. B **89**, 205311 (2014).

[42] R. Roldán, M. P. López-Sancho, F. Guinea, E. Cappelluti, J. A. Silva-Guillén, P. Ordejón, Momentum dependence of spin–orbit interaction effects in single-layer and multi-layer transition metal dichalcogenides, 2D Mater. **1,** 034003 (2014).

[43] J. He, K. Hummer, C. Franchini, Stacking effects on the electronic and optical properties of bilayer transition metal dichalcogenides MoS_2, $MoSe_2$, WS_2, and WSe_2, Phys. Rev. B **89,** 075409 (2014).

[44] A. Kuc, N. Zibouche, T. Heine, Influence of quantum confinement on the electronic structure of the transition metal sulfide TS_2, Phys. Rev. B **83,** 245213 (2011).

[45] J. K. Ellis, M. J. Lucero, G. E. Scuseria, The indirect to direct band gap transition in multilayered MoS_2 as predicted by screened hybrid density functional theory, Appl. Phys. Lett. **99**, 261908 (2011).

[46] A. Ramasubramaniam, D. Naveh, E. Towe, Tunable band gaps in bilayer transition-metal dichalcogenides, Phys. Rev. B **84,** 205325 (2011).

[47] A. Kumar, P. Ahluwalia, Electronic structure of transition metal dichalcogenides monolayers 1H-MX_2 (M= Mo, W; X= S, Se, Te) from ab-initio theory: new direct band gap semiconductors. Eur. Phys.l J. B **85**, 186 (2012).

[48] T. Chu, H. Ilatikhameneh, G. Klimeck, R. Rahman, Z. Chen, Electrically tunable bandgaps in bilayer MoS_2, Nano Lett. **15,** 8000 (2015).

[49] P. Lu, X. Wu, W. Guo, X. C. Zeng, Strain-dependent electronic and magnetic properties of MoS_2 monolayer, bilayer, nanoribbons and nanotubes, Phys. Chem. Chem. Phys. **14,** 13035 (2012).

[50] W. S. Yun, S. Han, S. C. Hong, I. G. Kim, J. D. Lee, Thickness and strain effects on electronic structures of transition metal dichalcogenides: 2H-MX_2 semiconductors (M= Mo, W; X= S, Se, Te), Phys. Rev. B **85,** 033305 (2012).

[51] E. Scalise, M. Houssa, G. Pourtois, V. Afanas'ev, A. Stesmans, Strain-induced semiconductor to metal transition in the two-dimensional honeycomb structure of MoS_2, Nano Res. **5,** 43 (2012).

[52] Q. Liu, L. Li, Y. Li, Z. Gao, Z. Chen, J. Lu, Tuning electronic structure of bilayer MoS_2 by vertical electric field: a first-principles investigation, J. Phys. Chem. C **116,** 21556 (2012).

[53] S. Bhattacharyya, A. K. Singh, Semiconductor-metal transition in semiconducting bilayer sheets of transition-metal dichalcogenides, Phys. Rev. B **86,** 075454 (2012).

[54] S. Han, H. Kwon, S. K. Kim, S. Ryu, W. S. Yun, D. H. Kim, J. H. Hwang, J.-S. Kang, J. Baik, H. J. Shin, S. C. Hong, Band-gap transition induced by interlayer van der Waals interaction in MoS_2, Phys. Rev. B **84,** 045409 (2011).

[55] F. Zahid, L. Liu, Y. Zhu, J. Wang, H. Guo, A generic tight-binding model for monolayer, bilayer and bulk MoS_2, AIP Adv. **3,** 052111 (2013).

[56] A. Molina-Sánchez, D. Sangalli, K. Hummer, A. Marini, L. Wirtz, Effect of spin-orbit interaction on the optical spectra of single-layer, double-layer, and bulk MoS_2, Phys. Rev. B **88,** 045412 (2013).

[57] H. Zeng, G-B. Liu, J. Dai, Y. Yan, B. Zhu, R. He, L. Xie, S. Xu, X. Chen, W. Yao, X. Cui, Optical signature of symmetry variations and spin-valley coupling in atomically thin tungsten dichalcogenides, Sci. Rep. **3,** 1608 (2013).

[58] D. Voß, P. Krüger, A. Mazur, J. Pollmann, Atomic and electronic structure of WSe_2 from ab initio theory: Bulk crystal and thin film systems, Phys. Rev. B **60**, 14311 (1999).

[59] P. E. Blöchl, Projector augmented-wave method, Phys. Rev. B **50,** 17953 (1994).

[60] G. Kresse, J. Furthmüller, Efficient iterative schemes for ab initio total-energy calculations using a plane-wave basis set, Phys. Rev. B **54,** 11169 (1996).

[61] J. P. Perdew, K. Burke, M. Ernzerhof, Generalized gradient approximation made simple, Phys. Rev. Lett.**77,** 3865 (1996).

[62] H. Zeng, B. Zhu, K. Liu, J. Fan, X. Cui, Q. Zhang, Low-frequency Raman modes and electronic excitations in atomically thin MoS_2 films, Phys. Rev. B **86,** 241301 (2012).

FIG. 1. (a) Top view of stick-and-ball hexagonal lattice structure of bilayer MoS_2. The blue and yellow spheres represent Mo and S atoms, respectively. (b) Trigonal prismatic coordination. (c) The first BZ of bilayer MoS_2 and critical points loci. (d) Optical micrograph of a representative bilayer MoS_2 sample. (e) AFM image of bilayer MoS_2. (f) Raman spectra of bilayer MoS_2 as compared with monolayer and trilayer MoS_2 under 2.33 eV excitation. The vibrational patterns of the corresponding E^1_{2g} and A_{1g} are illustrated in the insets.

FIG. 2. (a) Band structure of bilayer MoS_2 from first principle calculation with SOC. Fermi level is set to zero. (b) Mo-d orbitals (left) and total p orbitals (right) projected band structures of bilayer MoS_2. (c) and (d) Direct-gap (c) and indirect-gap (d) PL spectra at different temperatures. The indirect PL spectra of the I_1 and I_2 features are fitted to Lorentzians at 10 K. (e) Threshold energies of B exciton, A exciton and trion versus temperature. (f) Peak position of I_1 exciton and I_2 exciton as a function of temperature. (g) DFT calculations of energy spacing between K_c and K_{v1}/ K_{v2} versus temperature. (h) DFT calculations of energy spacing between Q_c/K_c and Γ_v versus temperature.

FIG. 3. (a), (c) and (e) The evolution of the energy difference between A and I_2 excitons (a), between I_1 and I_2 excitons (c) and between B and A excitons (e) as a function of temperature. (b), (d) and (f) DFT calculations of energy spacing between Γ_v and K_{v1} (b), between Q_c and K_c (c) and between K_{v1} and K_{v2} (d) versus temperature.

FIG. 4. (a) Schematic of highest splitting valence band at K valley due to SOC and LH in bilayer MoS_2. (b) and (c) DFT calculations of energy spacing between K_{v1} and K_{v2} versus the change of in plane lattice constant (b) and interlayer spacing (c).

FIG. 5. LH and layer polarization as a function of temperature. The layer polarization increases while LH decreases with increasing temperature.

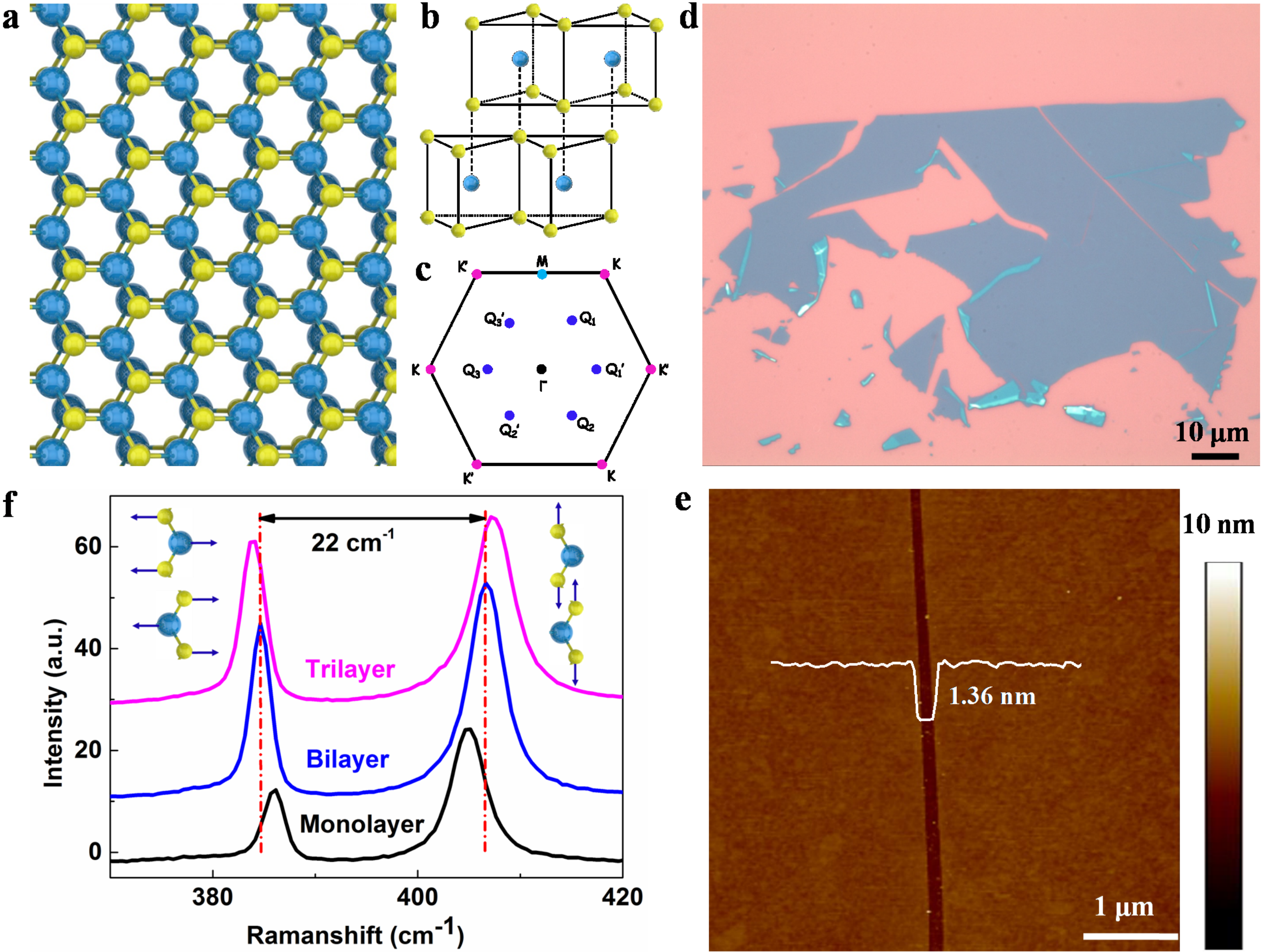
a
b
c
K'
M
K
Q3'
Q1
K
Q3
Γ
Q1'
K'
Q2'
Q2
K'
K
d
10 μm
f
22 cm-1
60
40
20
0
Trilayer
Bilayer
Monolayer
Intensity (a.u.)
380
400
420
Ramanshift (cm-1)
e
10 nm
1.36 nm
1 μm

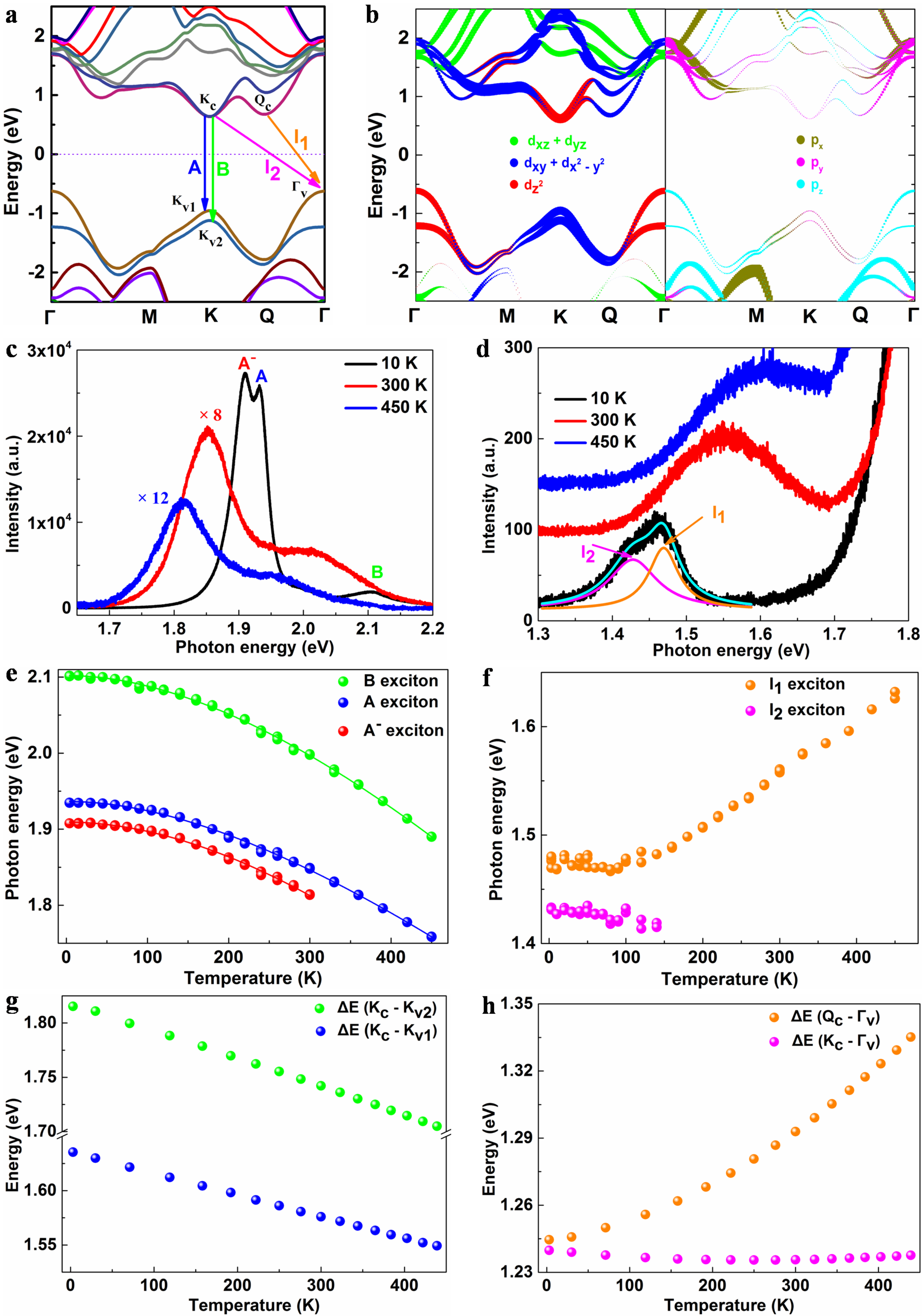
a
Energy (eV)
2
1
0
-1
-2
K_c
Q_c
A
B
I_1
I_2
K_v1
K_v2
Γ_v
Γ M K Q Γ
b
Energy (eV)
d_xz + d_yz
d_xy + d_x²-y²
d_z²
p_x
p_y
p_z
Γ M K Q Γ M K Q Γ
c
Intensity (a.u.)
3x10^4
2x10^4
1x10^4
0
10 K
300 K
450 K
A⁻
A
× 8
× 12
B
1.7 1.8 1.9 2.0 2.1 2.2
Photon energy (eV)
d
Intensity (a.u.)
300
200
100
0
10 K
300 K
450 K
I_1
I_2
1.3 1.4 1.5 1.6 1.7 1.8
Photon energy (eV)
e
Photon energy (eV)
2.1
2.0
1.9
1.8
B exciton
A exciton
A⁻ exciton
0 100 200 300 400
Temperature (K)
f
Photon energy (eV)
1.6
1.5
1.4
I_1 exciton
I_2 exciton
0 100 200 300 400
Temperature (K)
g
Energy (eV)
1.80
1.75
1.70
1.60
1.55
ΔE (K_c - K_v2)
ΔE (K_c - K_v1)
0 100 200 300 400
Temperature (K)
h
Energy (eV)
1.35
1.32
1.29
1.26
1.23
ΔE (Q_c - Γ_v)
ΔE (K_c - Γ_v)
0 100 200 300 400
Temperature (K)

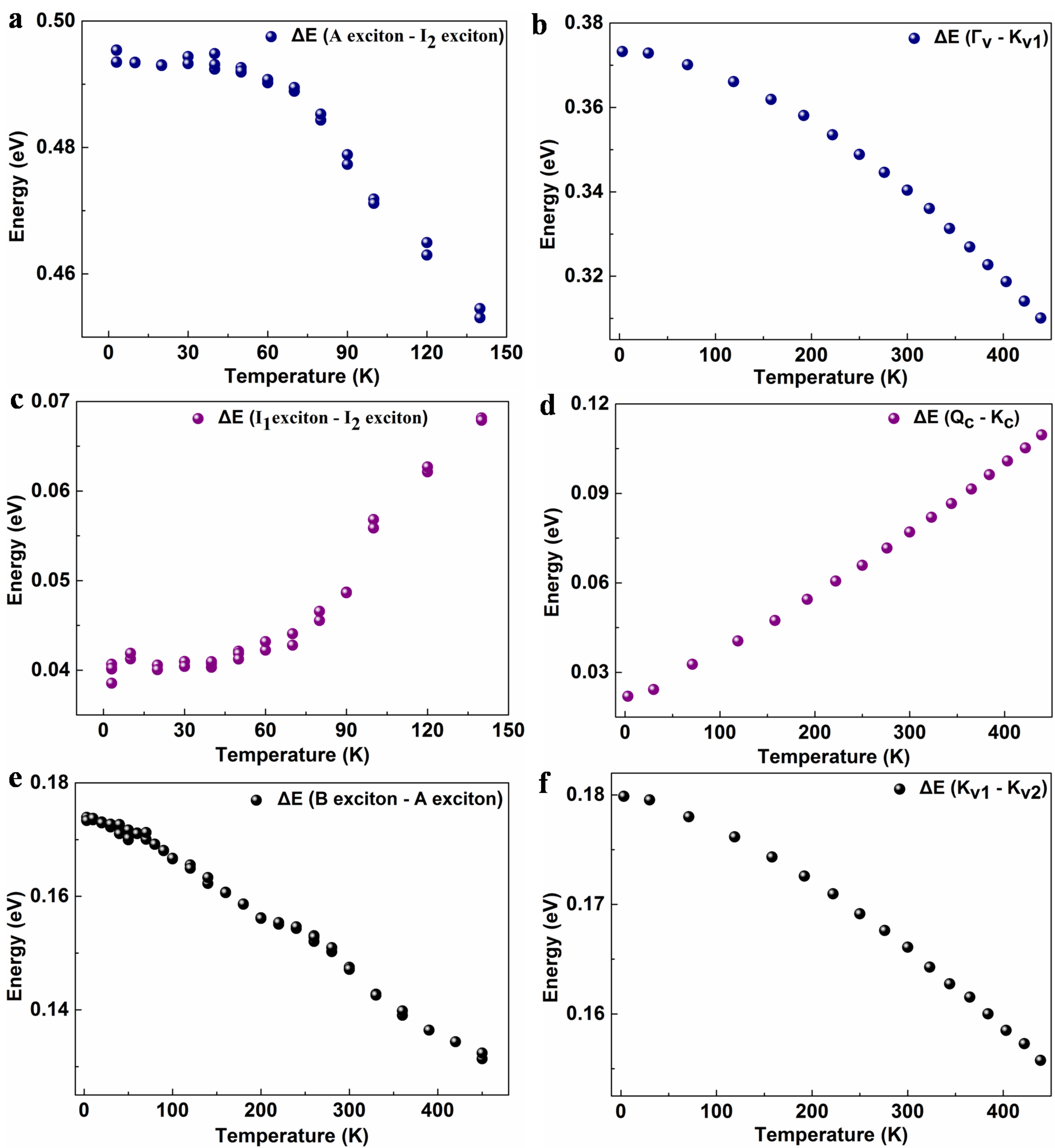
a
0.50
0.48
0.46
Energy (eV)
0
30
60
90
120
150
Temperature (K)
ΔE (A exciton - I_2 exciton)
b
0.38
0.36
0.34
0.32
Energy (eV)
0
100
200
300
400
Temperature (K)
ΔE (Γ_v - K_{v1})
c
0.07
0.06
0.05
0.04
Energy (eV)
0
30
60
90
120
150
Temperature (K)
ΔE (I_1exciton - I_2 exciton)
d
0.12
0.09
0.06
0.03
Energy (eV)
0
100
200
300
400
Temperature (K)
ΔE (Q_c - K_c)
e
0.18
0.16
0.14
Energy (eV)
0
100
200
300
400
Temperature (K)
ΔE (B exciton - A exciton)
f
0.18
0.17
0.16
Energy (eV)
0
100
200
300
400
Temperature (K)
ΔE (K_{v1} - K_{v2})

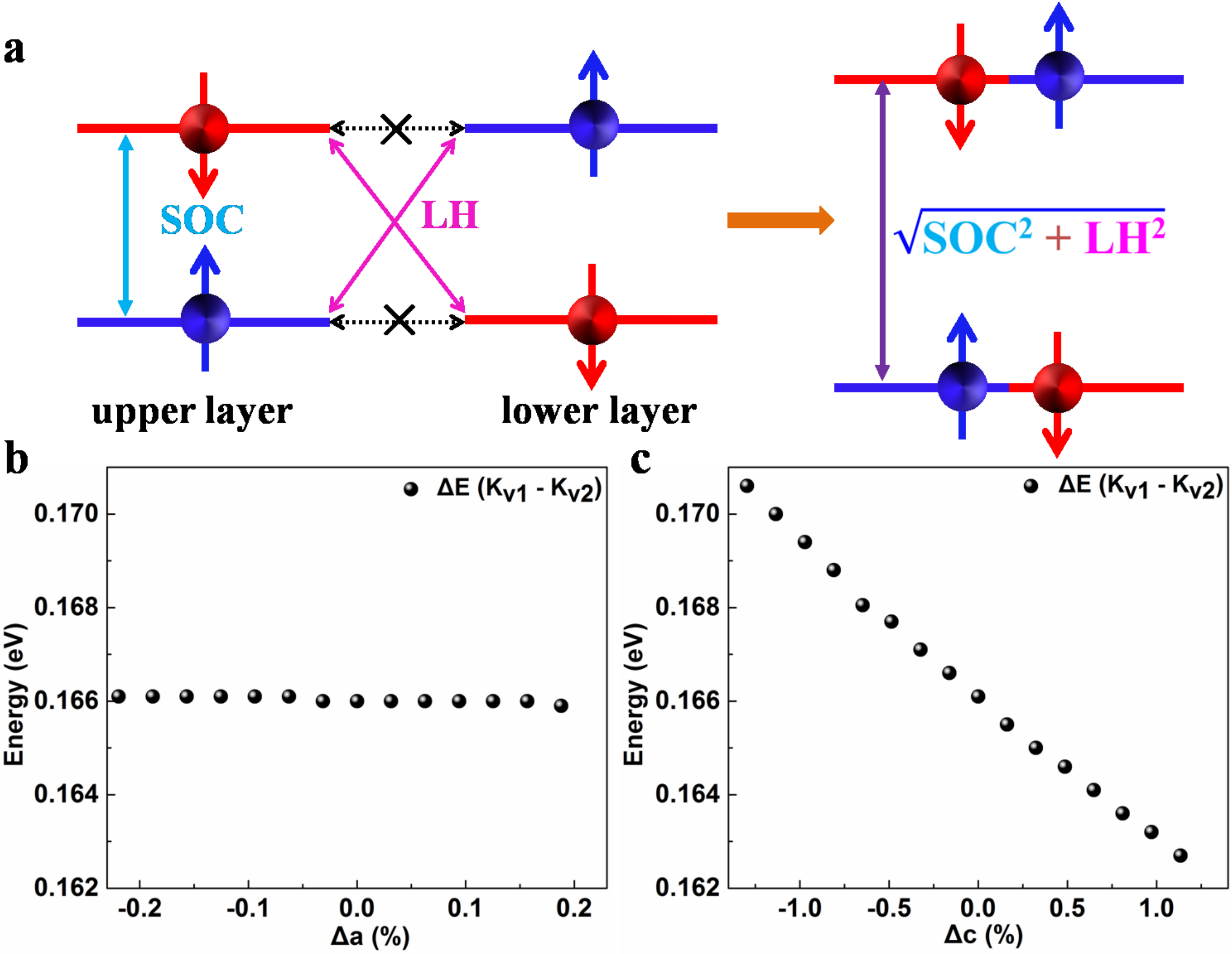
a
SOC
LH
upper layer
lower layer
$\sqrt{\mathrm{SOC}^2 + \mathrm{LH}^2}$
b
ΔE (K_{v1} - K_{v2})
Energy (eV)
0.162
0.164
0.166
0.168
0.170
-0.2
-0.1
0.0
0.1
0.2
Δa (%)
c
ΔE (K_{v1} - K_{v2})
Energy (eV)
0.162
0.164
0.166
0.168
0.170
-1.0
-0.5
0.0
0.5
1.0
Δc (%)

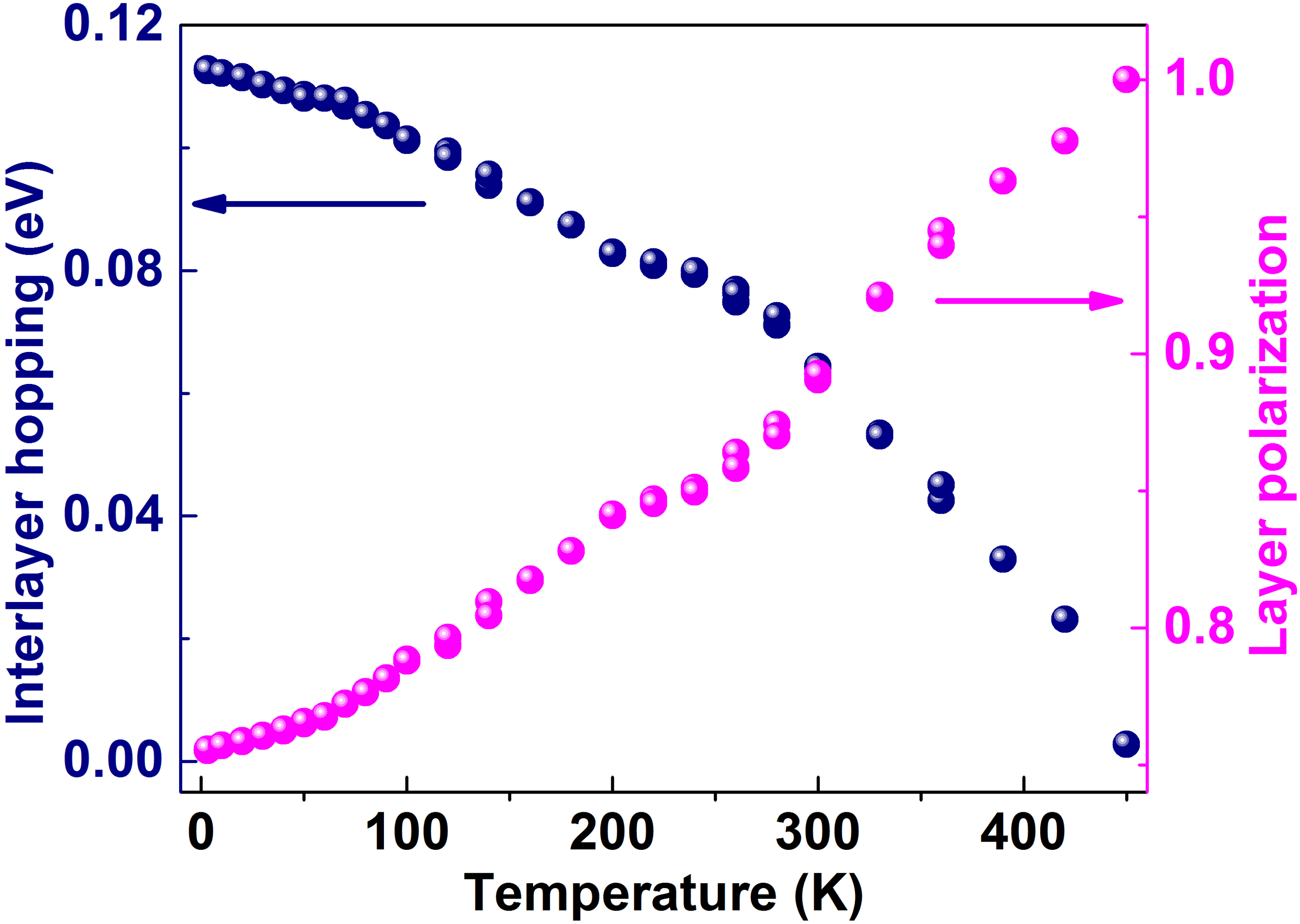
0.12
0.08
0.04
0.00
Interlayer hopping (eV)
1.0
0.9
0.8
Layer polarization
0
100
200
300
400
Temperature (K)